

Constraints on the Evolution of the Primordial Magnetic Field from the Small Scale CMB Angular Anisotropy

D. G. Yamazaki^{1,2}, K. Ichiki², T. Kajino^{2,1} and G. J. Mathews³

yamazaki@th.nao.ac.jp

ABSTRACT

Recent observations of the cosmic microwave background (CMB) have extended measured the power spectrum to higher multipoles $l \gtrsim 1000$, and there appears to be possible evidence for excess power on small angular scales. The primordial magnetic field (PMF) can strongly affect the CMB power spectrum and the formation of large scale structure. In this paper, we calculate the CMB temperature anisotropies generated by including a power-law magnetic field at the photon last scattering surface (PLSS). We then deduce an upper limit on the primordial magnetic field based upon our theoretical analysis of the power excess on small angular scales. We have taken into account several important effects such as reionization and the modified matter sound speed in the presence of a magnetic field. An upper limit to the field strength of $|B_\lambda| \lesssim 4.7$ nG at the present scale of 1 Mpc is deduced. This is obtained by comparing the calculated theoretical result including the Sunyaev-Zeldovich (SZ) effect with recent observed data on the small scale CMB anisotropies from the Wilkinson Microwave Anisotropy Probe (WMAP), the Cosmic Background Imager (CBI) and the Arcminute Cosmology Bolometer Array Receiver (ACBAR). We discuss several possible mechanisms for the generation and evolution of the PMF.

Subject headings: cosmology: cosmic microwave background — methods: numerical — magnetic field

¹Department of Astronomy, Graduate School of Science, University of Tokyo, 7-3-1 Hongo, Bunkyo-ku, Tokyo, 113-0033, Japan

²Division of Theoretical Astronomy, National Astronomical Observatory Japan, 2-21-1, Osawa, Mitaka, Tokyo, 181-8588, Japan

³Center for Astrophysics, Department of Physics, University of Notre Dame, Notre Dame, IN 46556, U.S.A.

1. Introduction

The possible existence of a primordial magnetic field (PMF) is an important question in modern cosmology. The PMF could influence a variety of phenomena in the early universe (Tsagas and Maartens 2000; Grasso and Rubinstein 2001; Betschart et al. 2003; Bruni et al. 2003; Clarkson et al. 2003; Giovannini 2004; Vallée 2004; Challinor 2005; Kahniashvili et al. 2005; Dolgov 2005; Kosowsky 2005; Gopal and Sethi 2005; Tashiro et al. 2005; Tashiro and Sugiyama 2005). However, there is still no firm understanding of the origin and evolution of the PMF, especially the observable magnetic field of $0.1 - 1.0 \mu\text{G}$ in galaxy clusters (Clarke et al. 2001; Xu et al. 2006). Recently, the origin of the PMF on such scales has been studied by a number of authors (Quashnock 1989; Boyanovsky et al. 2002; Bamba and Yokoyama 2004; Berezhiani and Dolgov 2004; Hanayama et al. 2005; Takahashi et al. 2005; Ichiki et al. 2006). There is, however, a possible discrepancy between theory and observation on the scale of galactic clusters. Temperature and polarization anisotropies in the CMB provide very precise information on the physical processes in operation during the early universe. However, the CMB data from the Wilkinson Microwave Anisotropy Probe (WMAP; Bennett, et al. 2003), the Arcminute Cosmology Bolometer Array Receiver (ACBAR; Kuo et al. 2004), and the Cosmic Background Imager (CBI; Mason et al. 2003) have indicated a potential discrepancy between the best-fit cosmological model to the WMAP data and observations at higher multipoles $l \geq 1000$. A straightforward extension of the fit to the WMAP data predicts a rapidly declining power spectrum in the large multipole range due to the finite thickness of the photon last scattering surface (PLSS). However, the ACBAR and CBI experiments indicate continued power up to $l \sim 4000$. This discrepancy is difficult to account for by a simple retuning of cosmological parameters.

One possible interpretation of such excess power at high multipoles is a manifestation of the re-scattering of CMB photons by hot electrons in clusters known as the thermal SZ effect (Sunyaev and Zeldovich 1980). Although there can be no doubt that some contribution from the SZ effect exists in the observed angular power spectrum, it has not yet been established conclusively that this is the only possible interpretation (Aghanim et al. 2001) of the small scale power. Indeed, the best value of the matter fluctuation amplitude, σ_8 to fit the excess power at high multipoles is near the upper end of the range of the values deduced by the other independent methods (Bond et al. 2005; Komatsu and Seljak 2002). Toward a solution of this problem, it has recently been proposed (Mathews et al. 2004) that a bump feature in the primordial spectrum may provide a better explanation for both the CMB and matter power spectra at small scales.

In this paper we consider another possibility. Inhomogeneous cosmological magnetic field generated before the CMB last-scattering epoch is also a plausible mechanism to pro-

duce excess power at high multipoles. Such a field excites an Alfvén-wave mode in the baryon-photon plasma in the early universe and induces small rotational velocity perturbations. Since this mode can survive on scales below those at which Silk damping occurs during recombination (Jedamzik et al. 1998; Subramanian and Barrow 1998a), it could be a new source of the CMB anisotropies on small angular scales. Analytic expressions for the temperature and polarization angular power spectra on rather larger angular scales ($l \leq 500$) by Mack et al. (2002) based upon the thin PLSS approximation have been derived for both vector and tensor modes. Subramanian and Barrow (2002) considered the vector perturbations in the opposite limit of smaller angular scales. Non-gaussianity in fluctuations from the PMF has also been considered (Brown and Crittenden 2005). A strong magnetic field in the early universe, however, may conflict with the cosmological observations currently available. The combination of those studies and current observations places a bound on the strength of the PMF of $B < 1.0 - 10$ nG.

In order to compare the CMB anisotropy induced by the PMF with observations more precisely, we need to perform numerical calculations of the fully linearized MHD equations along with a realistic recombination history of the universe. In particular, we first need to develop a numerical method to predict the theoretical spectrum for intermediate angular scales, in which the analytic approximation becomes inappropriate. Recently, efforts along this line have been done (Lewis 2004) to obtain numerical estimates of the effects of the PMF on the CMB. Also Yamazaki et al. (2005a) have proven numerically that the PMF is an important physical process for higher multipoles l . They have constrained an upper limit to the PMF of $B < 3.9$ nG, based upon a likelihood analysis of the data (Yamazaki et al. 2005b).

The WMAP data is very precise, but it does not extend to $l > 900$. The PMF, however, affects the CMB power spectrum for higher multipoles l (Yamazaki et al 2005b; Lewis 2004). Thus, one purpose of this paper is to place a new limit on the strength of the primordial magnetic field by comparing our calculated result with the WMAP, CBI and ACBAR data, the latter two of which have measured CMB anisotropies for higher multipoles l than WMAP. We will also discuss the consistency between our CMB constraints and the magnetic field in galactic clusters.

2. Primordial Stochastic Magnetic Field

Before recombination, Thomson scattering between photons and electrons along with Coulomb interactions between electrons and baryons were sufficiently rapid that the photon-baryon system behaves as a single tightly coupled fluid. Since the trajectory of plasma

particles is bent by Lorentz forces in a magnetic field, photons are indirectly influenced by the magnetic field through Thomson scattering. Let us consider the PMF created at some moment during the radiation-dominated epoch. The energy density of the magnetic field can be treated as a first order perturbation upon a flat Friedmann-Robertson-Walker (FRW) background metric. In the linear approximation, the magnetic field evolves as a stiff source. Therefore, we can discard all back reactions from the magnetohydrodynamic (MHD) fluid onto the field itself. The electromagnetic tensor has the usual form

$$F^\alpha{}_\beta = \begin{pmatrix} 0 & E_1 & E_2 & E_3 \\ E_1 & 0 & -B_3 & B_2 \\ E_2 & B_3 & 0 & -B_1 \\ E_3 & -B_2 & B_1 & 0 \end{pmatrix}, \quad (1)$$

where E_i and B_i are the electric and magnetic fields. Here we use natural units $c = \hbar = 1$. The energy momentum tensor for electromagnetism is

$$T^{\alpha\beta}{}_{[\text{EM}]} = \frac{1}{4\pi} \left(F^{\alpha\gamma} F_\gamma{}^\beta - \frac{1}{4} g^{\alpha\beta} F_{\gamma\delta} F^{\gamma\delta} \right). \quad (2)$$

The Maxwell stress tensor, σ^{ik} is derived from the space-space components of the electromagnetic energy momentum tensor,

$$-T^{ik}{}_{[\text{EM}]} = \sigma^{ik} = \frac{1}{a^2} \frac{1}{4\pi} \left\{ E^i E^k + B^i B^k - \frac{1}{2} \delta^{ik} (E^2 + B^2) \right\}. \quad (3)$$

Within the linear approximation (Durrer et al., 2000) we can discard the MHD back reaction onto the field itself. The conductivity of the primordial plasma is very large, and it is frozen-inh (Mack et al. 2002). This is a very good approximation during the epochs of interest here. Furthermore, we can neglect the electric field, i.e. $E \sim 0$, and can decouple the time evolution of the magnetic field from its spatial dependence, i.e. $\mathbf{B}(\tau, \mathbf{x}) = \mathbf{B}(\mathbf{x})/a^2$ for very large scales. In this way we obtain the following equations,

$$T^{00}{}_{[\text{EM}]} = \frac{B^2}{8\pi a^6}, \quad (4)$$

$$T^{i0}{}_{[\text{EM}]} = T^{0k}{}_{[\text{EM}]} = 0, \quad (5)$$

$$-T^{ik}{}_{[\text{EM}]} = \sigma^{ik} = \frac{1}{8\pi a^6} (2B^i B^k - \delta^{ik} B^2). \quad (6)$$

2.1. Two-Point Correlation Function

We assume that the PMF, \mathbf{B}_0 , deviates from a homogeneous and isotropic distribution in a statistically random way. The power spectrum of fluctuations from a homogeneous

and isotopic distribution can then be taken as a power-law $P(k) \propto k^{n_B}$ (Mack et al. 2002) where k is the wave number, and the spectral index n_B can be either positive or negative. Evaluating the two-point correlation function of the electromagnetic stress-energy tensor, we can obtain a good approximation to the the vector isotropic spectrum for $k < k_C$ (Mack et al. 2002)⁴,

$$|\Pi^{(1)}(\mathbf{k})|^2 \simeq \frac{1}{4(2n_B + 3)} \left[\frac{(2\pi)^{n_B+3} B_\lambda^2}{2\Gamma\left(\frac{n_B+3}{2}\right) k_\lambda^{n_B+3}} \right]^2 \times \left(k_C^{2n_B+3} + \frac{n_B}{n_B + 3} k^{2n_B+3} \right), \quad (7)$$

where the vector mode Lorentz force, $L(\mathbf{k})$, is given by $L(\mathbf{k}) = k\Pi^{(1)}(\mathbf{k})$, B_λ is the comoving mean magnetic-field amplitude obtained by smoothing over a Gaussian sphere of comoving radius λ , and $k_\lambda = 2\pi/\lambda$ (where $\lambda = 1$ Mpc in this paper). In this equation k_C is the cutoff wave number in the magnetic power spectrum defined by

$$k_C \simeq \left(5.08 \times 10^{-2} \times \frac{B_\lambda}{\text{InG}} \right)^{2/n_B+5} \times \left(\frac{k_\lambda}{1\text{Mpc}^{-1}} \right)^{\frac{n_B+3}{n_B+5}} (\Omega_b h^3)^{1/n_B+5}, \quad (8)$$

where h is the Hubble parameter in units of $100 \text{ km s}^{-1} \text{ Mpc}^{-1}$, (Mack et al. 2002; Jedamzik, et al. 1998; Subramanian and Barrow 1998a). Since the magnetic field source term $\Pi^{(1)}(\mathbf{k})$ depends quadratically on the magnetic field strength, the explicit time dependence of the magnetic stress is given by $\Pi(\tau, \mathbf{k}) = \Pi(\mathbf{k})/a^4$. The scalar mode of the magnetic field stress tensor $\Pi^{(0)}$ is obtained via a similar calculation (Koh and Lee 2002)

$$|\Pi^{(0)}(\mathbf{k})|^2 \simeq \frac{1}{2(2n_B + 3)} \left[\frac{(2\pi)^{n_B+3} B_\lambda^2}{2\Gamma\left(\frac{n_B+3}{2}\right) k_\lambda^{n_B+3}} \right]^2 \times \left(k_C^{2n_B+3} + \frac{n_B}{n_B + 3} k^{2n_B+3} \right). \quad (9)$$

⁴This has a form similar to that used in Mack et al. (2002) who treated two kinds of Fourier transforms of different normalizations. Here, we systematically adopt the same normalization for the Fourier transform. This removes the some of the uncertainty in the numerical calculations (Lewis 2004).

2.2. Ionization ratio

In previous studies the ionization ratio x_e in the early universe has been assumed to obey a step function in time, i.e. $x_e = 1$ before the PLSS and $x_e = 0$ after the PLSS. However, more accurate theoretical results require the use of the exact ionization ratio. We have therefore carried out a numerical estimate of the ionization ratio by using the program "RECFAST" (Seager et al. 1999). In this paper we take exact account of the ionization ratio $x_e(\tau)$, and can now rewrite the Lorentz force as

$$L(\tau, \mathbf{k}) = kx_e(\tau)\Pi^{(1)}(\mathbf{k}) \quad . \quad (10)$$

3. Perturbation Evolution Equations

To obtain the scalar and vector perturbation evolution equations we write the perturbed Einstein equation as

$$(\bar{G}_{\mu\nu} + \delta G_{\mu\nu}) = 8\pi G(\bar{T}_{\mu\nu[\text{FL}]} + \delta T_{\mu\nu[\text{FL}]}) \quad , \quad (11)$$

where $T_{\mu\nu[\text{FL}]}$ is the energy-momentum tensor of a perfect fluid. The Einstein equation can then be separated into background and perturbation equations. The background Einstein tensor is given by

$$\bar{G}_{\mu\nu} = \bar{R}^\mu{}_\nu - \frac{1}{2}\delta^\mu{}_\nu \bar{R} \quad , \quad (12)$$

while the perturbation tensor is

$$\delta G_{\mu\nu} = \delta R^\mu{}_\nu - \frac{1}{2}\delta^\mu{}_\nu \delta R \quad . \quad (13)$$

The perturbed Einstein equation is then

$$\delta R^\mu{}_\nu - \frac{1}{2}\delta^\mu{}_\nu \delta R = 8\pi G \delta T^\mu{}_\nu[\text{FL}] \quad . \quad (14)$$

The perfect fluid energy-momentum tensor has the form

$$T^\mu{}_\nu[\text{FL}] = p_{[\text{FL}]}g^\mu{}_\nu + (\rho_{[\text{FL}]} + p_{[\text{FL}]})U^\mu U_\nu \quad , \quad (15)$$

where the subscript $[\text{FL}]$ denotes the fluid, while $U^\mu = dx^\mu/\sqrt{-ds^2}$ is the four-velocity of the fluid relative to an observer in the frame in which the Einstein equation (14) is solved. The pressure p and energy density ρ of a perfect fluid at a given point are defined to be

that as measured by a comoving observer instantaneously at rest with respect to the fluid. For a fluid moving with a small coordinate velocity $v^i \equiv dx^i/d\tau$, v^i can be treated as a perturbation of the same order as $\delta\rho_{[\text{FL}]} = \rho_{[\text{FL}]} - \bar{\rho}_{[\text{FL}]}$, $\delta p_{[\text{FL}]} = p_{[\text{FL}]} - \bar{p}_{[\text{FL}]}$, where $\bar{\rho}_{[\text{FL}]}$ and $\bar{p}_{[\text{FL}]}$ are the background unperturbed state variables and τ is the proper time. Then, to linear order in the perturbations, the energy-momentum tensor is given by

$$T^0_{0[\text{FL}]} = -(\bar{\rho}_{[\text{FL}]} + \delta\rho_{[\text{FL}]}) \quad , \quad (16)$$

$$T^0_{i[\text{FL}]} = (\bar{\rho}_{[\text{FL}]} + \bar{p}_{[\text{FL}]})v_i = -T^i_{0[\text{FL}]} \quad , \quad (17)$$

$$T^i_{j[\text{FL}]} = (\bar{p}_{[\text{FL}]} + \delta p_{[\text{FL}]})\delta^i_j + \Sigma^i_j \quad , \quad \Sigma^i_i = 0 \quad . \quad (18)$$

Since we wish to consider the affect of the PMF, we combine the electromagnetic and perfect fluid energy momentum tensors,

$$T^{\alpha\beta} = T^{\alpha\beta}_{[\text{FL}]} + T^{\alpha\beta}_{[\text{EM}]} \quad . \quad (19)$$

3.1. Boltzmann equations

To evolve perturbations with the PMF, we start with the weak field Boltzmann equation;

$$\frac{d}{d\tau}\vec{T}(\tau, \vec{x}, \hat{n}) \equiv \frac{\partial}{\partial\tau}\vec{T} + n^i\nabla_i\vec{T} = \vec{C}[\vec{T}] + \vec{G}[h_{\mu\nu}] \quad , \quad (20)$$

which describes the evolution of the vector \vec{T} under the Thomson collisional term $C[\vec{T}]$ and gravitational redshift in a perturbed metric $G[h_{\mu\nu}]$ (Hu and White 1997).

As the radiation free streams, gradients in the distribution produce anisotropies. For example, as photons from different temperature regions intersect on their trajectories, the temperature difference is reflected in the angular distribution. This effect is represented in the Boltzmann equation (20) as a gradient term,

$$\hat{n} \cdot \nabla \longrightarrow i\hat{n} \cdot \vec{k} = i\sqrt{\frac{4\pi}{3}}kY_1^0, \quad (21)$$

which includes the intrinsic angular dependence of the temperature and polarization distributions, Y_l^m and ${}_{\pm 2}Y_l^m$, respectively. We utilize the following two Clebsch-Gordan relations:

$$\begin{aligned} ({}_{s_1}Y_{l_1}^{m_1}) ({}_{s_2}Y_{l_2}^{m_2}) &= \frac{\sqrt{(2l_2+1)(2l_1+1)}}{4\pi} \\ &\times \sum_{l,m,s} \langle l_1, l_2; m_1, m_2 | l_1, l_2; l, m \rangle \times \\ &\langle l_1, l_2; -s_1, s_2 | l_1, l_2; l, -s \rangle \sqrt{\frac{4\pi}{2l+1}} ({}_sY_l^m) \quad , \end{aligned} \quad (22)$$

and

$$\begin{aligned} \sqrt{\frac{4\pi}{3}} Y_1^0 ({}_s Y_l^m) = & \frac{{}_s \kappa_l^m}{\sqrt{(2l+1)(2l-1)}} ({}_s Y_{l-1}^m) - \frac{ms}{l(l+1)} ({}_s Y_l^m) \\ & + \frac{{}_s \kappa_{l+1}^m}{\sqrt{(2l+1)(2l+3)}} ({}_s Y_{l+1}^m) . \end{aligned} \quad (23)$$

Equation (23) couples multipoles l to the $l \pm 1$ moments of the distribution. Here, the coupling coefficient is

$${}_s \kappa_l^m = \sqrt{\frac{(l^2 - m^2)(l^2 - s^2)}{l^2}} . \quad (24)$$

The explicit form of the Boltzmann equations for the temperature and polarization follows directly from Clebsch-Gordan relations. For the moments of the temperature fluctuations $\Theta_l^{(m)}$ we have (Eq. (23) with $s = 0$),

$$\begin{aligned} \dot{\Theta}_l^{(m)} = k \left[\frac{{}_0 \kappa_l^m}{(2l-1)} \Theta_{l-1}^{(m)} - \frac{{}_0 \kappa_{l+1}^m}{(2l+3)} \Theta_{l+1}^{(m)} \right] \\ - \dot{\tau}_c \Theta_l^m + S_l^m (l \geq m) , \end{aligned} \quad (25)$$

where the source term $S_l^{(m)}$ accounts for the gravitational and residual scattering effects:

$$S_l^{(m)} = \begin{pmatrix} \dot{\tau}_c \Theta_0^{(0)} - \dot{\phi} & \dot{\tau}_c v_b^{(0)} + k\psi & \dot{\tau}_c P^{(0)} \\ 0 & \dot{\tau}_c v_b^{(1)} + \dot{V} & \dot{\tau}_c \dot{P}^{(1)} \\ 0 & 0 & \dot{\tau}_c P^{(2)} - \dot{H} \end{pmatrix} . \quad (26)$$

The presence of $\Theta_0^{(0)}$ in Eq. (26) represents the fact that the isotropic temperature fluctuations are not destroyed by scattering. The Doppler effect enters the dipole ($l = 1$) equation through the baryon velocity $v_b^{(m)}$ term.

In equations (25) and (26) we have introduced the optical depth τ_c between epoch τ and the present epoch τ_0 .

$$\tau_c(\tau) \equiv \int_{\tau}^{\tau_0} \dot{\tau}_c(\tau') d\tau' , \quad (27)$$

where, the combination $\dot{\tau}_c e^{-\tau_c}$ is the visibility function. It expresses the probability that a photon last scattered between τ and $\tau + d\tau$. Hence, this quantity is sharply peaked at the last scattering epoch.

The term in square brackets in equation (25) accounts for a free streaming effect that couples the l -modes to $l \pm 1$. This term implies that, in the absence of scattering, power is

transferred down the hierarchy when $k\tau \geq 1$. This transferal merely represents a geometrical projection of fluctuations on the scale corresponding to k at a distance τ which subtends an angle given by $l \sim k\tau$.

The main effect of scattering comes through the $\dot{\tau}_c \Theta_l^{(m)}$ term in Eq. (26). This term implies an exponential suppression of anisotropies with optical depth in the absence of sources.

Finally, the anisotropic nature of Compton scattering is expressed in Eq. (26) through

$$P^{(m)} = \frac{1}{10} [\Theta_2^{(m)} - \sqrt{6} E_2^{(m)}] . \quad (28)$$

These terms only involve the quadrupole moments of the temperature and E -polarization distributions.

The polarization evolution follows a similar derivation. Inserting $l \geq 2$, $m \geq 0$ into the Clebsch-Gordan relations of Eq. (23) with $s = \pm 2$ gives,

$$\begin{aligned} \dot{E}_l^{(m)} = k \left[\frac{2\kappa_l^m}{(2l-1)} E_{l-1}^{(m)} - \frac{2m}{l(l+1)} B_l^{(m)} - \frac{2\kappa_{l+1}^m}{(2l+3)} E_{l+1}^{(m)} \right] \\ - \dot{\tau}_c [E_l^m + \sqrt{6} P^{(m)} \delta_{l,2}] (l \geq m) , \end{aligned} \quad (29)$$

and

$$\begin{aligned} \dot{B}_l^{(m)} = k \left[\frac{2\kappa_l^m}{(2l-1)} B_{l-1}^{(m)} + \frac{2m}{l(l+1)} E_l^{(m)} - \frac{2\kappa_{l+1}^m}{(2l+3)} B_{l+1}^{(m)} \right] \\ - \dot{\tau}_c B_l^m (l \geq m) . \end{aligned} \quad (30)$$

3.2. Scalar Mode

We assume that the matter is representable as a perfect fluid and neglect the anisotropic pressure perturbations. We consider only adiabatic perturbations and neglect the entropy perturbations. The linearized perturbation equations which are obtained (Ma & Bertschinger, 1995; Hu & White, 1997; Koh & Lee, 2000) from the Einstein equations up to first order are:

$$3H^2\psi + 3H\dot{\phi} + k^2\phi = 4\pi Ga^2\delta T_0^0, \quad (31)$$

$$H\psi + \dot{\phi} = 4\pi Ga^2(\rho + p)v^{(0)}, \quad (32)$$

$$\ddot{\phi} + H(\dot{\psi} + 2\dot{\phi}) + \left(2\frac{\ddot{a}}{a} - H^2\right)\psi + \frac{k^2}{3}(\phi - \psi) = \frac{4\pi}{3}Ga^2\delta T_i^i, \quad (33)$$

$$k^2(\phi - \psi) = 12\pi Ga^2(\rho + p)\sigma, \quad (34)$$

where

$$\rho = \rho_{[\text{FL}]} + \rho_{[\text{EM}]}, \quad (35)$$

$$p = p_{[\text{FL}]} + p_{[\text{EM}]}, \quad (36)$$

while $v^{(0)}$ and σ are defined as

$$(\rho + p)v^{(0)} \equiv ik^j \delta T_j^0 \quad (37)$$

$$(\rho + p)\sigma \equiv - \left(\frac{\mathbf{k}_i \cdot \mathbf{k}_i}{k^2} - \frac{\delta_{ij}}{3} \right) \Sigma_j^i \quad (38)$$

and

$$\Sigma_j^i \equiv T_j^i - \frac{\delta_j^i T^k_k}{3} \quad (39)$$

denotes the traceless component of T_j^i . The conservation of energy-momentum is a consequence of the Bianchi identity;

$$T^{\mu\nu}{}_{;\mu} = \partial_\mu T^{\mu\nu} + \Gamma^\nu{}_{\alpha\beta} T^{\alpha\beta} + \Gamma^\alpha{}_{\alpha\beta} T^{\nu\beta} = 0 \quad (40)$$

Including the energy momentum tensor for the PMF and writing the magnetic energy density as

$$\rho_{[\text{EM}]} = \frac{B_\lambda^2}{2\pi}, \quad (41)$$

Eq. (40) leads to the following equations in k -space:

$$\dot{\delta} = -(1+w) \left(v^{(0)} - 3\dot{\phi} \right) - 3H \left(\frac{\delta p}{\delta \rho} - w \right) \delta \quad (42)$$

$$\dot{v}^{(0)} = -H(1-3w)v^{(0)} - \frac{\dot{w}}{1+w}v^{(0)} + \frac{\delta p}{\delta \rho} \frac{k^2 \delta}{1+w} - k^2 \sigma + k^2 \psi \quad (43)$$

where $w \equiv p/\rho$. Here, we can cancel $\sigma_{[\text{EM}]}$ in Eq. (43) in the linear perturbation limit. Thus, in the motion and continuity equations for the scalar mode, we can just add the energy density and pressure of the PMF to the general energy density and pressure respectively. From equations (42) and (43) we obtain the same form for the evolution equations of photons and baryons as that deduced in previous works (Ma & Bertschinger 1995; Hu & White 1997).

$$\dot{\delta}_\gamma = -\frac{4}{3}v_\gamma^{(0)} - 4\dot{\phi} \quad (44)$$

$$\dot{v}_\gamma^{(0)} = k^2 \left(\frac{1}{4}\delta_\gamma - \sigma_\gamma \right) + k^2 \psi + an_e \sigma_T (v_b^{(0)} - v_\gamma^{(0)}) \quad (45)$$

$$\dot{\delta}_b = -v_b^{(0)} + 3\dot{\phi} \quad (46)$$

$$\dot{v}_b^{(0)} = -\frac{\dot{a}}{a}v_b^{(0)} + c_s^2 k^2 \delta_b + \frac{4\bar{\rho}_\gamma}{3\bar{\rho}_b} an_e \sigma_T (v_\gamma^{(0)} - v_b^{(0)}) + k^2 \psi \quad (47)$$

where n_e is the free electron density, σ_T is the Thomson scattering cross section, and σ_γ in the second term on the right hand side of equation (45) is the shear stress of the photon with the PMF. In the presence of the PMF, the magnetic pressure should be included in the acoustic term. Therefore, the sound speed in the second term on the right hand side of Eq.(47) should be

$$c_s^2 = c_{bs}^2 + x_e(\tau)\Pi^{(0)}/4\pi a^4\rho_b, \quad (48)$$

where $x_e(\tau)$ is ionization ratio (we have solved x_e by using the RECFAST code (31)) and c_{bs} is the baryon sound speed without the PMF (see Adams et al 1996).

3.3. Vector Mode

The evolution of the vector potential $V(\tau, \mathbf{k})$ under the influence of the stochastic PMF can be written (Hu and White 1997; Mack et al. 2002) as

$$\begin{aligned} \dot{V}(\tau, \mathbf{k}) + 2\frac{\dot{a}}{a}V(\tau, \mathbf{k}) = & -\frac{16\pi GL^{(1)}(\tau, \mathbf{k})}{a^2k^2} \\ & -8\pi Ga^2\frac{p_\gamma\pi_\gamma + p_\nu\pi_\nu}{k}, \end{aligned} \quad (49)$$

where the dot denotes a conformal time derivative, p_i and π_i are the pressure and the anisotropic stress of the photons ($i = \gamma$) and neutrinos ($i = \nu$). Here, we have omitted the vector anisotropic stress of the plasma which is negligible in general. In the absence of a magnetic source term, the homogeneous solution of Eq. (49) behaves $V \propto 1/a^2$. We take $a \propto \tau$ during the radiation-dominated epoch. The magnetic field therefore causes the vector perturbations to decay less rapidly ($\propto 1/a$ instead of $1/a^2$) with the universal expansion.

Since the vector perturbations cannot generate density perturbations, we have $\delta_\gamma^{(1)} = \delta_b^{(1)} = 0$, where $\delta_\gamma^{(1)}$ and $\delta_b^{(1)}$ are the perturbations of the photon and baryon energy densities, respectively.

The magnetic field affects the photon-baryon fluid dynamics via a Lorentz force term in the baryon Euler equations. Following Hu and White (1997), the Euler equations for neutrino, photon and baryon velocities, v_ν , v_γ , and v_b are written as

$$\dot{v}_\nu^{(1)} - \dot{V} = -k \left(\frac{\sqrt{3}}{5} \Theta_{\nu 2}^{(1)} \right), \quad (50)$$

$$\dot{v}_\gamma^{(1)} - \dot{V} + \dot{\tau}_c(v_\gamma^{(1)} - v_b^{(1)}) = -k \left(\frac{\sqrt{3}}{5} \Theta_{\gamma 2}^{(1)} \right), \quad (51)$$

$$\dot{v}_b^{(1)} - \dot{V} + \frac{\dot{a}}{a}(v_b^{(1)} - V) - R\dot{\tau}_c(v_\gamma^{(1)} - v_b^{(1)})$$

$$= \frac{L^{(1)}(\tau, \mathbf{k})}{a^4(\rho_b + p_b)} , \quad (52)$$

where $R \equiv (\rho_\gamma + p_\gamma)/(\rho_b + p_b) \simeq (4/3)(\rho_\gamma/\rho_b)$ is the inertial density ratio between baryons and photons, while $\Theta_{\nu 2}^{(1)}$ and $\Theta_{\gamma 2}^{(1)}$ are quadrupole moments of the neutrino and photon angular distributions, respectively. These quantities are proportional to the anisotropic stress tensors. Equations (50)-(52) denote the vector equations of motion for the cosmic fluid, which arise from the conservation of energy-momentum.

4. Temperature Power Spectra

We follow the total angular momentum representation introduced by Hu and White (1997) to compute the CMB power spectra induced by the stochastic PMF. A transparent description of the CMB anisotropy formation can be obtained by combining the intrinsic angular structure with that of the plane-wave spatial dependence. Each moment corresponds directly to an observable angular sky pattern via an integral solution of the Boltzmann equations. We have constructed a Boltzmann code for the vector mode by explicitly expanding CMBFAST (Seljak & Zaldarriaga 1997). The temperature transfer function of the CMB today for the scalar and vector mode is expressed as an integral along the line of sight for $l \geq 2$

$$\frac{\Theta_l^{(0)}(\tau_0, k)}{2l+1} = \int_0^{\tau_0} d\tau e^{-\tau_c} [(\dot{\tau}_c \Theta_0^{(0)} + \dot{\tau}_c \psi + \dot{\psi} - \dot{\phi}) j_l^{(00)} + \dot{\tau}_c v_b^{(0)} j_l^{(10)} + \dot{\tau}_c P^{(0)} j_l^{(20)}] , \quad (53)$$

$$\frac{\Theta_l^{(1)}(\tau_0, k)}{2l+1} = \int_0^{\tau_0} d\tau e^{-\tau_c} \left\{ [\dot{\tau}_c (v_b^{(1)} - V)] D_1 \frac{j_l(x)}{x} + \left(\dot{\tau}_c P^{(1)} + \frac{\sqrt{3}}{3} kV \right) D_2 \frac{d}{dx} \left(\frac{j_l(x)}{x} \right) \right\} , \quad (54)$$

where the $j_l(x)$ are the spherical Bessel functions with $x = k(\tau_0 - \tau)$, $D_1 = \sqrt{l(l+1)}/2$, $D_2 = \sqrt{3}D_1$, and $P^{(1)}$ is the polarization term (Hu and White 1997). Using $\Theta_l^{(1)}(\tau_0, k)$, we can compute angular power spectrum of temperature anisotropies:

$$C_l^{(0)} = \frac{4}{\pi} \int dk k^2 \frac{|\Theta_l^{(0)}(\tau_0, k)|^2}{(2l+1)^2} , \quad (55)$$

$$C_l^{(1)} = \frac{4}{\pi} \int dk k^2 \frac{|\Theta_l^{(1)}(\tau_0, k)|^2}{(2l+1)^2} . \quad (56)$$

This power spectrum of temperature anisotropies is to be added to that induced by the scalar density perturbations and compared with observational data.

5. Result and Discussions

We discuss the effects of scalar and vector modes of the PMF and also the SZ effect on the CMB in this section. Note that the current data for higher l are known to be insensitive to the tensor mode which we ignored in the present calculations. Figures 1 and 2 show the CMB power spectra generated by the PMF. The effects of the PMF become progressively more important at higher multipoles and eventually dominates over the scalar fluctuations for $l > 1000$. As a result, the potential discrepancy between the observed and theoretical CMB temperature anisotropies at higher multipoles l is remarkably relaxed by the effects of the presence of a PMF (Yamazaki et al 2005). In the following subsections we discuss details on the behavior of the effects of the PMF on the CMB temperature anisotropies.

5.1. Scalar and Vector modes

The left hand side of Figure 1 shows the temperature anisotropies of the CMB power spectra which are generated by the PMF, and the right side hand of Figure 1 shows the primary temperature anisotropies calculated in the Λ Cold Dark Matter (LCDM) model with and without the effects of the PMF. The scalar part of the primary temperature anisotropies consists of several different sources of metric perturbations including photon and neutrino energy density perturbations as well as the perturbation due to the PMF. Therefore, the scalar mode generated by the PMF, as displayed by the green dash-dotted curves on the left hand side of Fig. 1, is evaluated by subtracting the two calculated CMB power spectra with and without the PMF in the LCDM model. Note that there is no such complication for the vector part of the primary temperature anisotropies because it arises uniquely from the vector mode of the PMF.

Both scalar and vector modes become larger with increasing field strength $|B_\lambda|$ of the PMF, but the variation of the vector mode is much stronger than the scalar mode (see the right hand side of Fig. 1). The scalar mode for the PMF gets complicated as is to be discussed later in this subsection. However the net effect is basically caused by two contributions: First, the increase of the sound speed for additional magnetic pressure to reduce baryonic matter fluctuation amplitude; and second, the changes of the metric and the total energy density which offset the first effect. Since the effect of the PMF for the vector mode is just an increase of the perturbation by the Lorentz force, the vector-to-scalar mode ratio increases as the strength of the PMF $|B_\lambda|$ increases.

The PMF affects both the energy density and pressure in the scalar mode. The influence on the energy density is the same as that on the baryon density. The magnetic pressure,

however, increases the sound speed of the fluid as discussed below Eqs.(46) and (47). This produces interesting effects on the CMB (Adams et al 1996; Tsagas and Maartens 2000; Yamazaki et al 2006). In order to understand the effects of the change of the sound speed, c_s , boosted by the PMF let us solve Eqs.(46) and (47) in the WKB approximation

$$\delta_b \propto -\frac{1}{\sqrt{c_s(\tau)a(\tau)}} \exp\left(-i \int c_s k d\tau\right). \quad (57)$$

This solution clearly shows two different influences of the change of c_s on the baryonic matter fluctuation: First, the increase of the sound speed due to the magnetic pressure results in a decrease in the amplitude of the evolution of δ_b because of the prefactor of Eq.(57). This means that in the presence of a magnetic field, the plasma pressure increases by the repulsion of lines of magnetic force. Thus, gravitational collapse of the matter is delayed. Second, increasing the sound velocity makes the frequency of the baryonic fluctuation δ_b larger because of the exponent of Eq.(57). This effect of the PMF on density field makes different kinds of amplitude boosts which depend on k (Yamazaki et al. 2006). The PMF shifts the acoustic oscillation for the baryon fluid either up or down depending on the combination of the sound speed c_s and wavenumber k . Note, however, that since the amplitude of the PMF is so small, the difference between the shifted and non-shifted period of the acoustic oscillations essentially only depends on the wavenumber k . This effect is strongly constrained by the observed data as displayed on the right hand side of Figure 1.

When one compares the scalar and vector modes, the scalar mode makes only a minor contribution to the CMB except at lower amplitudes. However, since the magnetic field pressure delays the gravitational collapse of matter, its effect on the matter power spectrum for large scale structure (LSS) is very interesting. Since in the present article we are only interested in the small scale structure associated with larger multipoles l , further details on this point will be discussed elsewhere (Yamazaki et al. 2006).

5.2. Dependence on B_λ

The CMB power spectrum generated by a cosmological magnetic field is generally characterized by a broad peak at $l \simeq 1000 \sim 3000$ for a reasonable range of $-2 < n_B \lesssim 0$ as shown in Fig. 2. We display five cases of the CMB power spectra for $B_\lambda = 1, 2, 4, 8,$ and 10 nG in Fig.1. As mentioned above, for lower l and B_λ , the scalar mode dominates (bottom three cases for $B_\lambda = 1, 2$ and 4 nG of the left hand side of Fig.1). For higher l and B_λ , the vector mode dominates. The amplitude is shown to increase with increasing magnetic field strength B_λ for $l > 1000$, where the vector mode dominates. Some lengthy mathematical derivation

of the power spectrum of fluctuations leads to $C_l \propto B_\lambda^4$ for $n_B < -3/2$, and $C_l \propto B_\lambda^{14/(n_B+5)}$ for $n_B > -3/2$ for higher multipoles l (Fig. 2).

5.3. Dependence on n_B

Fig. 2 shows the n_B dependence of the CMB. For $n_B < -3/2$, the second term in Eq.(7) dominates. This k -dependence causes a strong angular dependence for the vector mode perturbation. This results in changing the peak position for different multipoles l depending upon the power-law spectral index n_B . On the other hand, peaks remain at nearly the same multipole $l \sim 2000$ independently of n_B for $n_B > -3/2$. This is because the vector mode perturbation from the magnetic field tends to be that of white noise when the first term in Eq.(7) dominates.

6. Constraint on the PMF in a MCMC Analysis

To set limits on the PMF we have evaluated likelihood functions for fits to the WMAP, ACABAR, and CBI data over a wide range of the parameters, B_λ and n_B , for a stochastic PMF along with the usual six cosmological parameters, h , $\Omega_b h^2$, $\Omega_m h^2$, n_s , A_s , and τ_c . The quantity h is the Hubble constant in units of $100 \text{ km s}^{-1} \text{ Mpc}^{-1}$. The quantities $\Omega_b h^2$ and $\Omega_m h^2$ are the usual present baryon and cold dark matter closure parameters. The quantities n_s and A_s are the spectral index and the amplitude of the primordial scalar fluctuation, respectively. The parameter τ_c is the optical depth. We adopt a flat cosmology. To explore this parameter space, we have employed the Markov chain technique (Lewis 2002). We also take account of the SZ effect in our analysis. For that, we adopt a fixed prior of $\sigma_8 = 0.9$ (Spergel et al. 2003; Komatsu and Seljak 2002).

6.1. Degeneracy

In our likelihood analysis of the magnetic field parameters, we continued the MCMC algorithm until the cosmological parameters well converged to the values listed in Table 1. The inferred parameter values are consistent with those deduced in other analyses (Spergel et al. 2002; Mason et al., 2003; Kuo et al., 2004). We did not find obvious degeneracies of the magnetic field parameters with other cosmological parameters. We understand this for the following reasons. The primordial magnetic field is constrained (Jedamzik et al. 1998; Mack et al. 2002) by the cutoff scale for the damping of Alfvén waves as indicated by Eq. (8).

Since this cutoff scale is small compared with the multipoles for the currently available data at $l \ll 3000$, the manifestation of this effect is remarkably seen as a monotonically increasing contribution from both scalar and vector perturbations in the multipole region higher than $l \sim 500$ (Yamazaki et al. 2005a). This sensitivity of the CMB power spectrum to the primordial magnetic field differs completely from those to the other cosmological parameters, which helps resolve the degeneracies among them. There is, however, a strong degeneracy between the magnetic field strength $|B_\lambda|$ and the power spectral index n_B because those parameters affect the amplitude simultaneously [see Eqs. (7) and (9)].

6.2. Limits on the PMF

In Fig. 3 we show results of our MCMC analysis using the WMAP, ACBAR and CBI data in the two parameter plane $|B_\lambda|$ vs. n_B . The 1σ (68%) and 2σ (95.4%) C.L. excluded regions are bounded above by the thick curves as shown. We could not find a lower boundary of the allowed region at the 1σ or 2σ confidence level. Note, however, that we find a very shallow minimum with a reduced $\chi^2 \simeq 1.08$. From Fig. 3 we obtain an upper limit to the strength of the PMF at the 1σ (95.4%) C.L. of

$$|B_\lambda| \lesssim 7.7 \text{ nG at 1Mpc} . \quad (58)$$

This upper limit is particularly robust as we have considered all effects on the CMB anisotropies, i.e. the effect of the ionization ratio, the SZ effect, and the effects from both the scalar and vector modes on the magnetic field, in the present estimate of $|B_\lambda|$ and n_B .

7. PMF Generation and Evolution

In this section we discuss a multiple generation and evolution scenario of the cosmological primordial magnetic field that is motivated by the results of the present study.

To begin with we adopt the following three constraint conditions:

1. A PMF strength $|B_\lambda| \lesssim 7.7 \text{ nG}(1\sigma)$ at 1Mpc as deduced above by applying the MCMC method to the WMAP, ACBAR, and CBI data.
2. The magnetic field strength in galaxy clusters is $0.1\mu\text{G} < |B_{CG}| < 1\mu\text{G}$ (Clarke et al. 2001; Xu et al. 2006). Hence, if the isotropic collapse is the only process which amplifies the magnetic field strength, the lower limit to the PMF is $\sim 1 - 10$ nG for the PLSS.

3. The gravity wave constraint on the PMF from Caprini and Durrer (2002)⁵. The big-bang nucleosynthesis of the light elements depends on a balance between the particle production rates and the expansion rate of the universe. Since the energy density of the gravity waves ρ_{GW} contributes to the total energy density. However, ρ_{GW} is constrained so that the expansion rate of the universe does not spoil the agreement between the theoretical and observed light element abundance constraints for deuterium, ^3He , ^4He , and ^7Li (Maggiore, 2000).

Figures 3 and 4 summarize the various constraints on the PMF by these three conditions. The region bounded by the upper red-solid curve is constrained by condition (i) as indicated, the green-dash-dotted horizontal line corresponds to the lower limit to the PMF from condition (ii), and the Black-solid, sky-blue-dotted, and pink-dashed lines, respectively, are the upper limit of the produced PMF from big-bang nucleosynthesis, the electroweak transition, and the inflation epoch. Figure. 4 shows the allowed or excluded regions according to these multiple constraints depending upon when the PMF was generated:

(A). Nucleosynthesis: I+II+III region

$$\begin{aligned} 1.0 \text{ nG} &\lesssim |B_\lambda| \lesssim 4.7\text{nG} \\ -3 &\lesssim n_B \lesssim -2.40 \end{aligned}$$

(B). Electroweak transition: II+III region

$$\begin{aligned} 1.0 \text{ nG} &\lesssim |B_\lambda| \lesssim 4.7\text{nG} \\ -3 &\lesssim n_B \lesssim -2.43 \end{aligned}$$

(C). Inflation: III region

$$\begin{aligned} 1.0 \text{ nG} &\lesssim |B_\lambda| \lesssim 4.7\text{nG} \\ -3 &\lesssim n_B \lesssim -2.76 \end{aligned}$$

Obviously, the upper limits on both $|B_\lambda|$ and n_B become more stringent if the PMF is produced during an earlier epoch. Moreover, the limits we deduce are the strongest constraints on the PMF that have yet been determines. However, we caution that the evolution of the generation of the PMF during the LSS epoch is not well understood. Thus,

⁵ λ in Caprini and Durrer (2004) is for a scale of 0.1 Mpc, however our λ is for 1Mpc. Thus, inclinations of lines in Figs. 3 and 4 are smaller than Caprini and Durrer (2004).

if there are other effective physical processes for the generation and evolution of the PMF during the formation of LSS, our lower limit of the PMF parameters may decrease. In order to constrain the PMF parameters accurately, we should study the PMF not before but after the PLSS.

8. Conclusion

For the first time we have studied scalar mode effects of the PMF on the CMB. We have confirmed numerically without approximation that the excess power in the CMB at higher l can be explained by the existence of a PMF. For the first time a likelihood analysis utilizing the WMAP, ACBAR and CBI data with a MCMC method has been applied to constrain the upper limit on the strength of the PMF to be

$$|B_\lambda| < 7.7nG \quad .$$

We have also considered three conditions on the generation and evolution of the cosmological PMF: 1) our result; 2) the lower limit of the PMF from the magnetic field of galaxy clusters; and 3) the constraint on the PMF from gravity waves. Combining these, we find the following concordance region for the the PMF parameters;

$$1 \text{ nG} < |B_\lambda| < 4.7 \text{ nG} \quad , \quad -3.0 < n_B < -2.4 \quad .$$

The PMF also affects the formation of large scale structure. For example, magnetic pressure delays the gravitational collapse. It is thus very important to constrain the PMF as precisely as possible. If we combine our study and future plans to observe the CMB anisotropies and polarizations for higher multipoles l , e.g. via the *Planck Surveyor*, we will be able to constrain the PMF more accurately, and explain the evolution and generation of the magnetic field on galaxy cluster scales along with the formation of the LSS.

We acknowledge Drs. K. Saigo, H. Hanayama, M. Higa, R. Nakamura, K. Umezu, H. Ohno, K. Takahashi, M. Oguri, Prof. M. Yahiro for their valuable discussions. This work has been supported in part by Grants-in-Aid for Scientific Research (13640313, 14540271) and for Specially Promoted Research (13002001) of the Ministry of Education, Science, Sports and Culture of Japan, and the Mitsubishi Foundation. K. I. also acknowledges the support by Grant-in-Aid for JSPS Fellows. Work at the University of Notre Dame (G.J.M.) supported by the U.S. Department of Energy under Nuclear Theory Grant DE-FG02-95-ER40934.

A. Tight Coupling Approximation

Since the Thomson opacity is larger before recombination, photons and baryons are tightly coupled. If the Thomson drag terms in Eq.(45), (47), (51), and (52) are too large, it is difficult to solve these equations. Therefore, we here derive approximation equations in this limit. The tight coupling approximation for the scalar mode was introduced by Ma and Rertschinger (1997). Here, therefore, we only need to introduce the vector mode in this appendix.

Using equations (51) and (52), we obtain the following equations for the photons and baryons in the tight-coupling approximation.

$$\dot{v}_b^{(1)} = \frac{1}{1+R} \left(-\frac{\dot{a}}{a} v_b^{(1)} - R(\dot{v}_\gamma^{(1)} - \dot{v}_b^{(1)}) - \frac{\sqrt{3}}{5} k R \Theta_{\gamma^2}^{(1)} + \frac{L^{(1)}}{a^4(\rho_b + p_b)} \right) , \quad (\text{A1})$$

$$v_b^{(1)} - v_\gamma^{(1)} = \frac{1}{\dot{\tau}_c} \left(\dot{v}_\gamma^{(1)} + \frac{\sqrt{3}}{5} k \Theta_{\gamma^2}^{(1)} \right) . \quad (\text{A2})$$

Writing $\dot{v}_\gamma^{(1)}$ as $\dot{v}_b^{(1)} + (\dot{v}_\gamma^{(1)} - \dot{v}_b^{(1)})$, we can rewrite (A2)

$$v_b^{(1)} - v_\gamma^{(1)} = \frac{1}{\dot{\tau}_c} \left(\dot{v}_b^{(1)} + (\dot{v}_\gamma^{(1)} - \dot{v}_b^{(1)}) + \frac{\sqrt{3}}{5} k \Theta_{\gamma^2}^{(1)} \right) , \quad (\text{A3})$$

and using equations (A1) and (A2), we get

$$v_b^{(1)} - v_\gamma^{(1)} = \frac{1}{(1+R)\dot{\tau}_c} \left(-\frac{\dot{a}}{a} v_b^{(1)} + (\dot{v}_\gamma^{(1)} - \dot{v}_b^{(1)}) + \frac{\sqrt{3}}{5} k \Theta_{\gamma^2}^{(1)} + \frac{L^{(1)}}{a^4(\rho_b + p_b)} \right) . \quad (\text{A4})$$

Differentiating Eq. (A4) and ignoring terms of more than second order in $\dot{\tau}_c$, we get

$$\begin{aligned} \dot{v}_b^{(1)} - \dot{v}_\gamma^{(1)} &= \frac{\dot{a}}{a} \frac{2R}{(1+R)} (v_b^{(1)} - v_\gamma^{(1)}) \\ &+ \frac{1}{(1+R)\dot{\tau}_c} \left[-\frac{\ddot{a}}{a} v_b^{(1)} \right] \\ &+ O(\dot{\tau}_c^{-2}) . \end{aligned} \quad (\text{A5})$$

Substituting Eq. (A4) into Eq. (A1) yields

$$\dot{v}_\gamma^{(1)} = \frac{1}{R} \left[-\dot{v}_b^{(1)} - \frac{\dot{a}}{a} v_b^{(1)} - \frac{\sqrt{3}}{5} k R \Theta_{\gamma^2}^{(1)} + \frac{L^{(1)}}{a^4(\rho_b + p_b)} \right] . \quad (\text{A6})$$

REFERENCES

- Aghanim, N., Górski, K. M., Puget, J. L., 2001, *A&A*, 374, 1
- Bamba, K. & Yokoyama, J., 2004, *Phys. Rev. D* **70**, 083508
- Banerjee, R. and Jedamzik, K. 2004, *Phys. Rev. D* **70**, 123003
- Bennett, C. L., et.al., 2003, *ApJS*, 148, 1
- Berezhiani, Z. and Dolgov, A. D., 2004, *Astropart. Phys.* 21, 59
- Betschart, G., Dunsby, P. K. S., and Marklund, M., 2004, *Class. Quant. Grav.* **21**, 2115
- Bond, J. R. et al., 2005, *ApJ*, 626 12
- Brown, I. and Crittenden, R., 2005, *Phys. Rev. D* 72, 063002
- Bruni, M., Maartens, R. and Tsagas, C. G. 2003, *Mon. Not. Roy. Astron. Soc.* **338**, 785
- Boyanovsky, D., Simionato, M., and Vega, H. J. de, 2003, *Phys. Rev. D* **67**, 023502
- Caprini, C. & Durrer, R., 2002, *Phys. Rev. D*, 65, 023517
- Challinor, A., 2005 [astro-ph/0502093]
- Clarke, T. E., Kronberg, P. P. and Bohringer, H., 2001, *ApJL*, L111, 547
- Clarkson, C. A., Coley, A. A., Maartens, R., and Tsagas, C. G., 2003, *Class. Quant. Grav.* **20**, 1519
- Dolgov, A. D., 2005 [astro-ph/0503447]
- Gopal, R. and Sethi, S. K., 2005, *PRD*, 72, 103003
- Giovannini, M., 2004, *Phys. Rev. D* **70**, 123507
- Grasso, D., and Rubinstein, H. R., 2001, *Phys. Rept.* **348**, 163
- Hanayama, H., et al., 2005, *ApJ*. 633, 941
- Hu, W., & White, M., 1997, *Phy. Rev. D.*, 56, 596
- Ichiki, K., et al., 2006, *Science*, in press.
- Kahniashvili, T. and Ratra, B., 2005; *Phys. Rev. D* **71**, 103006

- Koh, S. and Lee, C. H., 2000, Phys. Rev. D, 62, 083509
- Komatsu, E., & Seljak, U., 2002, MNRAS, 336, 1256
- Kosowsky, A., Kahniashvili, T., Lavrelashvili, G. and Ratra, B., 2005, Phys. Rev. D **71**, 043006
- Kuo, C.L., et al., 2004, ApJ, 600, 32
- Jedamzik, K., Katalinic, V. and Olinto, A.V., 1998, Phys. Rev. D., 57, 3264
- Lewis, A., 2002, Phys. Rev. D, 66, 103511
- Lewis, A., 2004, Phys. Rev. D, 70, 043011
- Ma, C. P. & Bertschinger, E., 1995, ApJ. 455, 7
- Mack, A., Kahniashvili, T., & Kosowsky, A., 2002, Phys. Rev. D. 65, 123004
- Maggiore, M., 2000, [gr-qc/0008027]
- Mason, B. S., et al., 2003, ApJ, 591, 540
- Mathews, G. J., et al., 2004, Phys. Rev. D70, 083505
- Quashnock, J. M. Loeb, A., and Spergel, D. N. 1989, ApJL, 344, L49
- Seager, S., Sasselov, D., & Scott, D., 1999, ApJ, 523, L1
- Seljak, U., & Zaldarriaga, M., 1996, ApJ, 469, 437
- Spergel, D. N., et al., 2003, ApJS, 148, 175
- Subramanian, K., & Barrow, J. D., 1998a, Phys. Rev. D, 58, 083502
- Subramanian, K., & Barrow, J. D., 1998b, Phys. Rev. Lett. 81, 3575
- Subramanian, K., & Barrow, J. D., 2002, MNRAS, 335, L57
- Subramanian, K., Seshadri, T. R., & Barrow, J. D., 2003, MNRAS, 344, L31
- Sunyaev, R., & Zeldovich, I. B., 1980, ARA&A, 18, 537
- Takahashi, K. Ichiki, K., Ohno, H., and Hanayama, H., 2005, Phys. Rev. Lett. **95**, 121301
- Tashiro, H., Sugiyama, N., and Banerjee, R., 2005, Phys. Rev. D73, 023002

- Tashiro,H., Sugiyama,N.,2005, [astro-ph/0512626]
- Tsagas, C., Maartens, R., 2000, Phys.Rev. D61, 083519
- Vallée, J. P., 2004, New Astronomy Reviews, 48, 763
- Verde, L. et al., 2003, ApJS, 148, 195V
- Yamazaki, D. G., Ichiki, K., & Kajino, T., 2005a, Nucl. Phys. A 758, 791c
- Yamazaki, D. G., Ichiki, K., & Kajino, T., 2005b, ApJL. 625, L1
- Yamazaki, D. G., Hanayama, H., & Ichiki, K., 2006, submitted to Phys. Rev. D
- Xu, Y., Kronberg, P. P., Habib, S. and Dufton, Q. W., 2006, ApJ, 637, 19

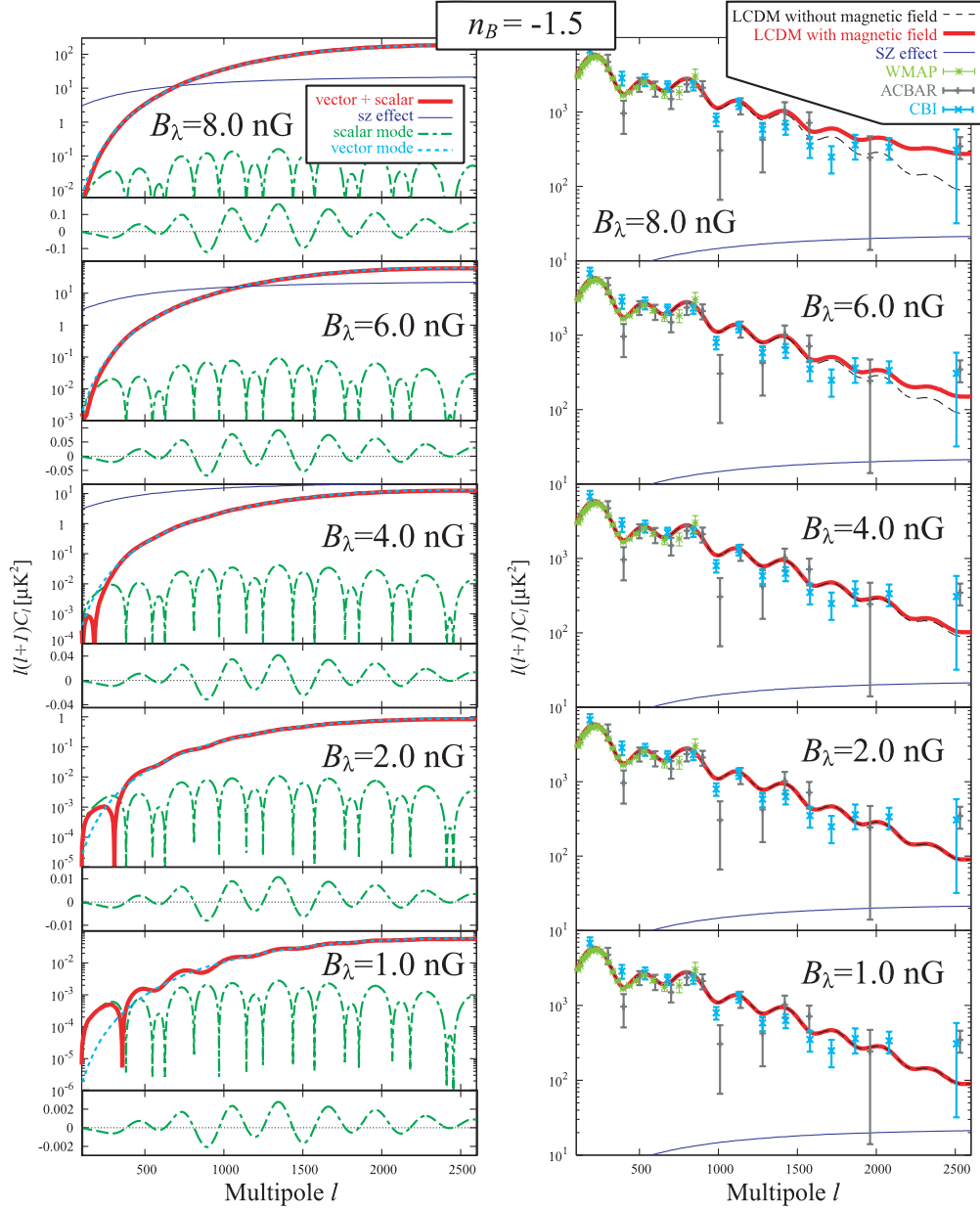


Fig. 1.— Effects of the PMF strength $|B_\lambda|$ on the CMB. The five figures on the left hand side show the CMB temperature anisotropies from the PMF. The red bold curves are the temperature anisotropies from vector and scalar modes of the PMF. The green dashed-dotted curves are for the scalar mode, the skyblue dotted curves are for the vector mode, and the purple thin curves show the SZ effect. The upper parts of the figures show the combined effects on the CMB. The lower parts show the effects of the scalar mode obtained by subtracting the LCDM model without the PMF from the LCDM model with the PMF. The five figures on the right hand side show the primary temperature anisotropies of the CMB with and without the PMF. The black short-dashed curves show the LCDM model without the PMF. The red bold curves are the LCDM model with the PMF. The purple thin curves are the SZ effect. The dots with lightgreen, gray, and skyblue error bars are the WMAP, ACBAR and CBI data, respectively. On all figures, the power spectral index of the PMF is set to $n_B = -1.5$. Also, the strengths of the PMF on both sides of this figure

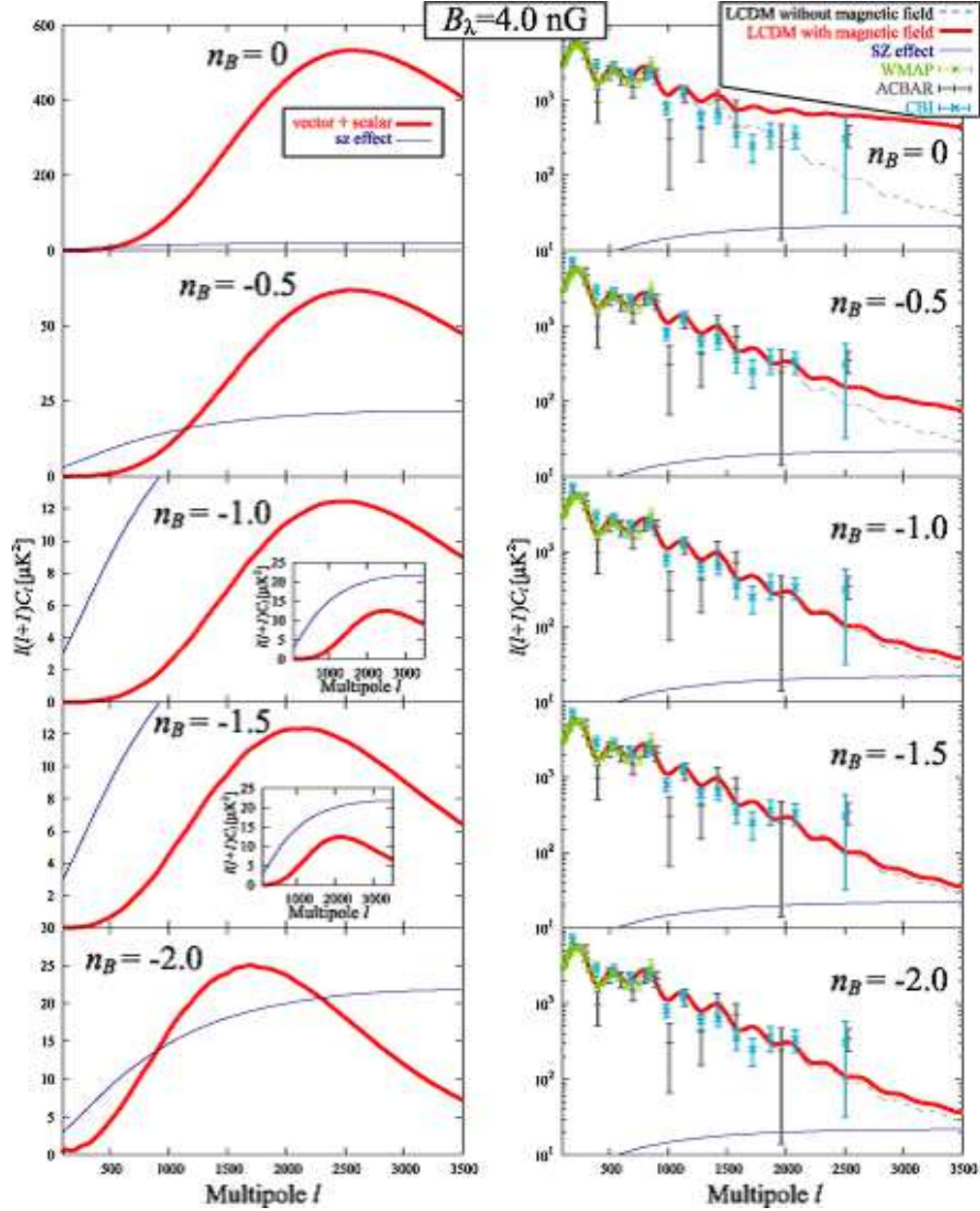


Fig. 2.— Effects power spectral index n_B of the PMF on the CMB. The five figures on the left hand side show the temperature anisotropies of the CMB from the PMF, and the red bold curves are the temperature anisotropies from the vector and scalar modes of the PMF. The purple thin curves show the SZ effect adopted here. The five figures on right hand side show the primary temperature anisotropies of the CMB with and without the PMF. The black short-dashed curves are the LCDM model without the PMF. The red bold curves are the LCDM model with the PMF. The purple thin curves are the SZ effect. The dots with lightgreen, gray, and skyblue error bars are WMAP, ACBAR and CBI data, respectively. On all figures, the strength of the PMF is set to be $|B_\lambda| = 4.0$ nG. Also the power spectral index of the PMF on both sides of this figure are set to $n_B = 0, -0.5, -1.0, -1.5,$ and -2.0 from top to bottom as labeled.

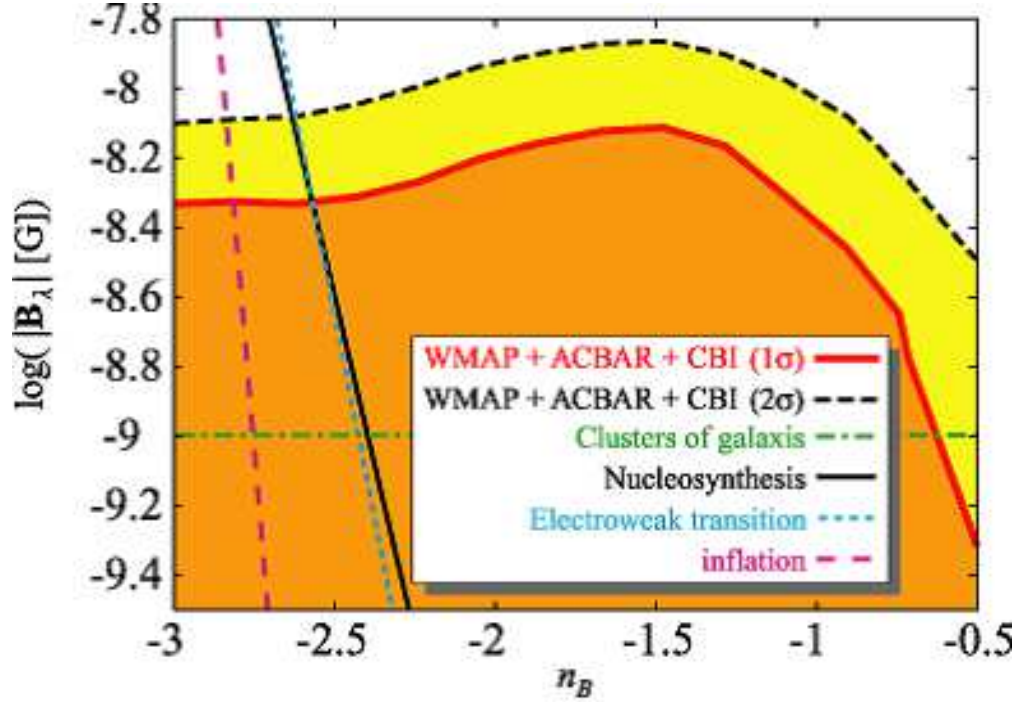


Fig. 3.— Results of the MCMC method constrained by the WMAP, ACBAR, and CBI data. Excluded and allowed regions at the 1σ (68%) C.L. and 2σ (95.4%) C.L. are shown in the two parameter plane of $|\mathbf{B}_\lambda|$ vs. n_B , where $|\mathbf{B}_\lambda|$ is the primordial magnetic field strength and n_B is the power-law spectral index. Solid and dotted curves are for $\Delta\chi^2 = 2.3$ and 6.17, respectively. The green dash-dotted horizontal line displays the lower limit of the field strength $B_\lambda = 1$ nG deduced for the galaxy cluster scale at the PLSS (Clarke, et al 2001; Xu, et al 2006). The black-solid, skyblue-dotted, and pink-dashed lines are the upper limit of the produced PMF at the big-bang nucleosynthesis, the electroweak transition, and the inflation epochs, respectively (Caprini and Durrer 2002).

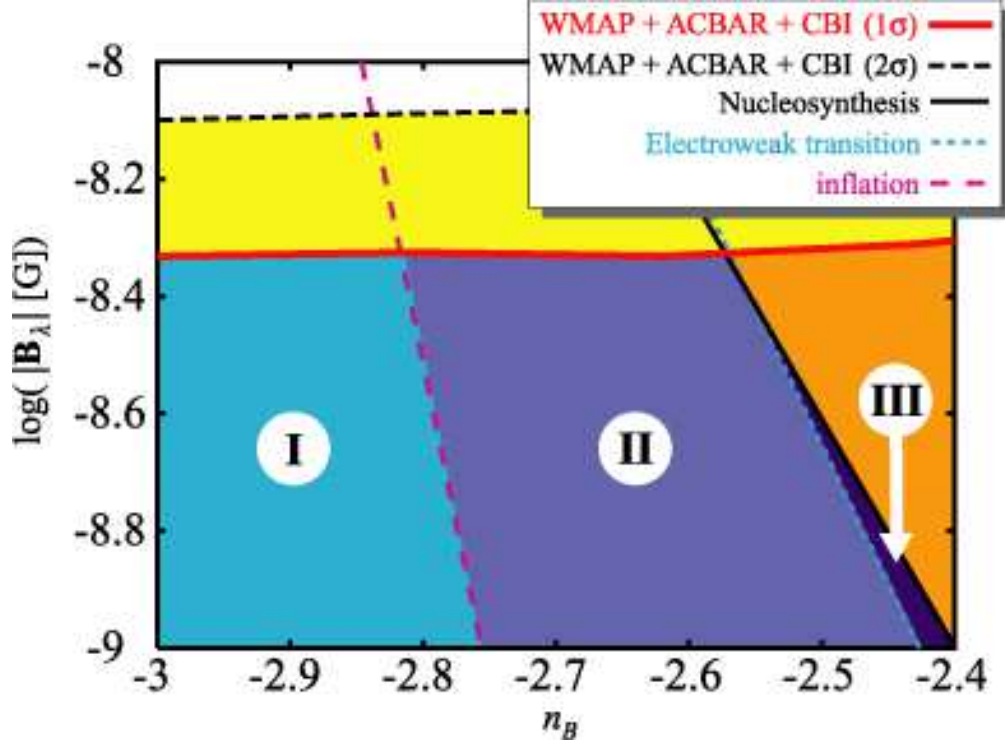


Fig. 4.— Excluded and allowed regions at the 1σ (68%) C.L. and 2σ (95.4%) C.L. in the two parameter plane $|\mathbf{B}_\lambda|$ vs. n_B obtained by the MCMC method with the WMAP, ACBAR, and CBI data. $|\mathbf{B}_\lambda|$ is the primordial magnetic field strength and n_B is the power-law spectral index. The solid and dotted curves are for $\Delta\chi^2 = 2.3$ and 6.17, respectively. The black-solid, skyblue-dotted, and pink-dashed lines are the upper limit of the produced PMF at the big-bang nucleosynthesis, the electroweak transition, and the inflation epochs, respectively (Caprini and Durrer 2002). If the PMF is produced at the epochs of big-bang nucleosynthesis, the electroweak transition, or inflation, respectively, the region of I+II+III, II+III, or III are allowed by these constraints on the PMF for the galaxy cluster scale at the PLSS and the MCMC method with WMAP, ACBAR, and CBI data.

Table 1. Calculated LCDM model parameters which best fit the WMAP data with the effect of primordial magnetic field taken into account.

Parameter	Mean and 68% C.L. Errors	95% C.L. Errors
$\Omega_b h^2$	$0.0231^{+0.0011}_{-0.0010}$	$+0.0021$ -0.0020
$\Omega_{CDM} h^2$	$0.120^{+0.011}_{-0.011}$	$+0.024$ -0.018
n_s	$0.976^{+0.027}_{-0.026}$	$+0.054$ -0.046
A_s	$0.903^{+0.131}_{-0.129}$	$+0.236$ -0.194
τ_c	$0.126^{+0.034}_{-0.039}$	$+0.11$ -0.10
h	$0.727^{+0.037}_{-0.037}$	$+0.074$ -0.070

Note. — Calculated corresponding cosmic expansion ages are $t_0/\text{Gyr} = 13.35^{+0.21}_{-0.21}$ (68% C.L.) and $13.35^{+0.41}_{-0.41}$ (95% C.L.).